AIP | Review of Scientific Instruments

Laboratory-based x-ray reflectometer for multilayer characterization in the 15–150 keV energy band

David L. Windt

Citation: Review of Scientific Instruments **86**, 043107 (2015); doi: 10.1063/1.4916737
View online: http://dx.doi.org/10.1063/1.4916737
View Table of Contents: http://scitation.aip.org/content/aip/journal/rsi/86/4?ver=pdfcov
Published by the AIP Publishing

Laboratory-based x-ray reflectometer for multilayer characterization in the 15–150 keV energy band

David L. Windt[a)]
Reflective X-ray Optics LLC, 1361 Amsterdam Ave., Suite 3B, New York, New York 10027, USA

(Received 5 February 2015; accepted 23 March 2015; published online 8 April 2015)

A laboratory-based X-ray reflectometer has been developed to measure the performance of hard X-ray multilayer coatings at their operational X-ray energies and incidence angles. The instrument uses a sealed-tube X-ray source with a tungsten anode that can operate up to 160 kV to provide usable radiation in the 15–150 keV energy band. Two sets of adjustable tungsten carbide slit assemblies, spaced 4.1 m apart, are used to produce a low-divergence white beam, typically set to 40 μm × 800 μm in size at the sample. Multilayer coatings under test are held flat using a vacuum chuck and are mounted at the center of a high-resolution goniometer used for precise angular positioning of the sample and detector; additionally, motorized linear stages provide both vertical and horizontal adjustments of the sample position relative to the incident beam. A CdTe energy-sensitive detector, located behind a third adjustable slit, is used in conjunction with pulse-shaping electronics and a multi-channel analyzer to capture both the incident and reflected spectra; the absolute reflectance of the coating under test is computed as the ratio of the two spectra. The instrument's design, construction, and operation are described in detail, and example results are presented obtained with both periodic, narrow-band and depth-graded, wide-band hard X-ray multilayer coatings. [http://dx.doi.org/10.1063/1.4916737]

INTRODUCTION

Nanometer-scale multilayer coatings have been developed in recent years to provide high reflectance at grazing incidence for X-ray energies above 10 keV. These new coatings have been used in applications including X-ray optics for synchrotron instrumentation and hard X-ray telescopes for astronomy.[1–5] Research is on-going to develop improved hard X-ray multilayer coatings that provide even higher reflectance and operate at ever-greater X-ray energies.[6–8]

The successful development of new X-ray multilayer coating technology requires accurate characterization of both film structure and X-ray performance. Conventional thin-film characterization techniques, such as X-ray diffraction and low angle scattering (i.e., typically using monochromatic radiation at 8 keV from a copper sealed-tube or rotating anode X-ray source), high-resolution transmission electron microscopy, atomic force microscopy, and other surface analysis techniques, remain instrumental in the development of such coatings, providing detailed information on film microstructure, interface properties, surface roughness, and so forth. However, the absolute reflectance of the coating at the operational X-ray energies and incidence angles, so-called "at-wavelength" performance, is a crucially important attribute of any optical multilayer coating, including those designed for the hard X-ray band, and its measurement provides invaluable feedback during coating development. In many cases, hard X-ray reflectance measurements made as a function of photon energy are also required for absolute calibration of multilayer-coated mirrors and other optical elements used in the construction of complete instruments.

With few exceptions, past investigations of multilayer performance in the hard X-ray band have relied on synchrotron radiation facilities for at-wavelength characterization.[6–8] However, synchrotron beamlines dedicated to hard X-ray reflectometry do not exist at present, and there are constraints on the use of those beamlines that are suitable for hard X-ray reflectometry. That is, reflectance measurements at hard X-ray energies at synchrotron facilities have typically required significant advance planning for outside users, and a competitive selection process that allocates only limited beam-time, a significant portion of which must be expended for the setup of an *ad hoc* reflectometer end-station. This situation has led to a paucity of accurate, at-wavelength data on hard X-ray multilayers and has constrained their development.

To address the need for at-wavelength characterization during the development of new hard X-ray multilayer coatings, a dedicated, laboratory-based hard X-ray reflectometer has been created. The instrument builds on the approach described by Høghøj *et al.*[9] for the development of a laboratory-based hard X-ray reflectometer and was inspired by the development in recent years of various so-called "energy dispersive" X-ray reflectometers that utilize energy-sensitive detectors and no monochromators.[10–13] The reflectometer uses a sealed-tube X-ray source and tungsten carbide slits to create a low-divergence white pencil beam, and an energy-sensitive detector is used to record both the incident spectrum and the spectrum of X-rays reflected from a flat multilayer sample precisely positioned in the beam, at the desired incidence angle. The absolute multilayer reflectance as a function of energy is computed as the ratio of the two spectra. The instrument is easy to use and

a)davidwindt@gmail.com

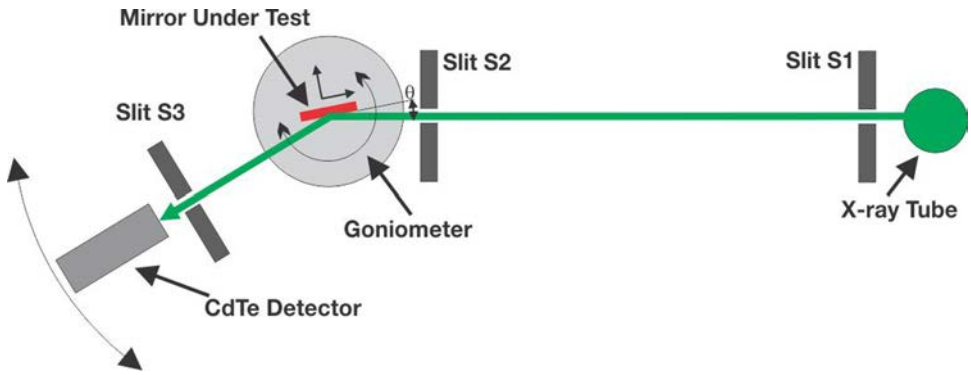

FIG. 1. Schematic diagram of hard X-ray reflectometer.

can provide rapid feedback during multilayer development, as well as absolute calibration data for working multilayer optics.

HARD X-RAY REFLECTOMETER DESIGN

A schematic diagram of the hard X-ray reflectometer is shown in Fig. 1; a photo and 3D CAD model of the system are shown in Fig. 2. The main components of the instrument are the X-ray tube, the three sets of slit assemblies (labeled S1, S2, and S3), the goniometer assembly, and the detector. The entire system is housed within custom-built radiation shielding.

The water-cooled X-ray tube is fitted with a tungsten anode (Comet[14] model no. MXR-160HP/11) and can be operated at tube voltages up to 160 kV. The tube can maintain 1800 W continuous power with a 1.0 mm focal spot or 800 W continuous power with a 0.4 mm focal spot. Typical X-ray spectra are shown in Fig. 3 and comprise tungsten K and L emission lines superposed on a broad Bremsstrahlung continuum extending up to the applied tube voltage, which is 160 kV in this example. The tube can also be operated at lower voltages with higher currents, in order to increase the X-ray flux at low energies as required for certain measurements.

The three slit assemblies shown in Figs. 1 and 2 each comprises a mechanism having two pair of 10-mm-thick tungsten carbide slit blades (JJ X-ray[15] model AT-F7-Air): in each assembly, one pair of slit blades is oriented vertically and the other horizontally. The center position of, and gap between, each pair of slit blades is independently adjustable, using small stepper motor and lead-screw combinations that provide 0.322 μm/full-step of center position displacement and 0.813 μm/full-step of gap displacement. Each pair of motorized slit blades is contained within a metal housing that is in turn mounted on a motorized gimbal mechanism for angular positioning of the slit-pair about an axis located at the center of the housing that is orthogonal to the direction of slit motion, i.e., either vertical or horizontal, and to the X-ray beam axis. The gimbal motion is used to ensure that the plane containing each pair of slit blades is precisely perpendicular to the X-ray beam axis. This orientation maximizes the flux of X-rays through the slit-pair even as the gap is set to tens of micrometer, as is needed for reflectometry at shallow graze angles (typically well below 1°) where a small beam footprint on the sample is required. The two slit blades that make up a pair travel along separate paths within the slit-pair housing, so the blades can be made to completely overlap and block the beam, in principle.

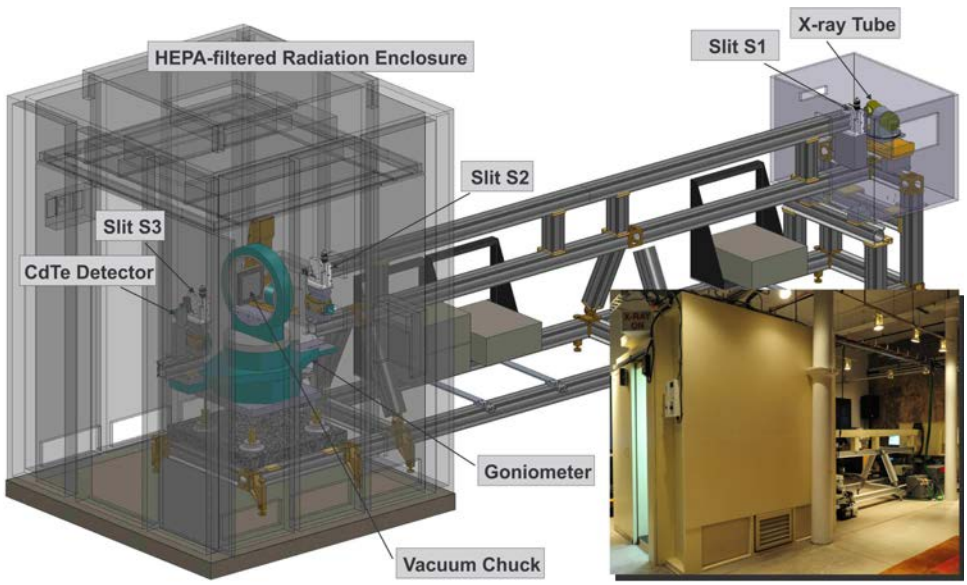

FIG. 2. 3D CAD model and photograph (inset) of the hard X-ray reflectometer system.

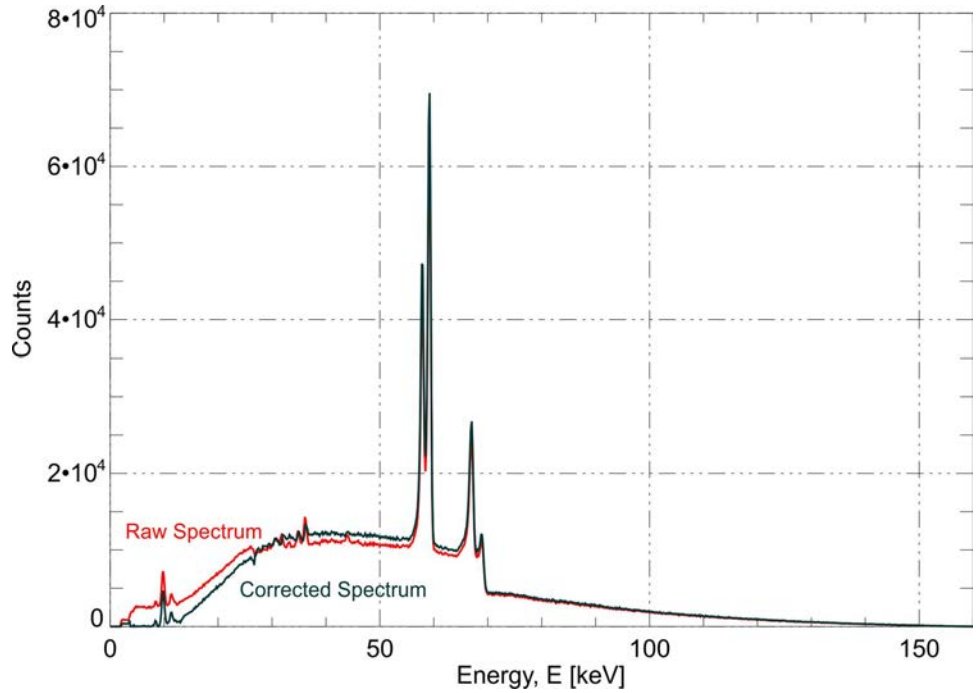

FIG. 3. Incident X-ray spectra, obtained with a tube voltage of 160 keV and an integration time of 15 min. Both the raw spectrum and the escape-peak-corrected spectrum (explained in the text) are shown.

The X-ray tube and the first slit assembly (S1) are both mounted in a custom-designed radiation enclosure (Energy Services and Bookholt Associates[16]) with a pivoting 3-piece lid, all constructed from lead-lined steel, as shown in Fig. 4. Safety interlocks prevent the X-ray tube from operating while the enclosure is open. The X-ray tube is mounted in a fixture that allows for manual adjustment of the angle of the tube relative to the beam propagation direction, in order to capture the brightest part of the $30° \times 40°$ cone beam emerging from the tube. The tube mounting fixture is in turn mounted on a motorized linear stage (Newport model[17] IMS-300) so that the focal spot can be precisely positioned relative to the slit when the tube angle is changed. To minimize scattering from slit assembly components that are otherwise illuminated by the X-ray cone-beam, a 6.4-mm-thick lead plate is located between the tube and the slit assembly, with a 12.7 mm diameter hole positioned in front of the entrance to the slit assembly.

The radiation enclosure that houses the tube and slit S1 is mounted on a structural support constructed from hollow, extruded aluminum beam sections and compatible mating parts for assembly and component mounting (Newport system X95). The X-ray beam emerging from slit S1 travels inside one such beam, which is enclosed in a radiation shroud constructed from lead and steel. The second slit assembly, S2, is mounted at the end of that beam, at a distance of 4.1 m from S1, inside a second, and much larger radiation enclosure that also houses the goniometer, the third slit (S3), and the detector. The X-ray tube, slits S1 and S2, and the shielded aluminum beam between the two slits are all mounted on a second aluminum beam; additional aluminum beams located along the base of the support structure extend further into the radiation enclosure and support the goniometer assembly as well. The rigid extruded aluminum beam structure facilitates system alignment and provides mechanical stability.

The two slits S1 and S2 define the extent and divergence of the X-ray beam incident on the sample under test. For example, with 40 μm horizontal slit widths, the horizontal beam divergence is ~0.001°. For the case of flat test sample

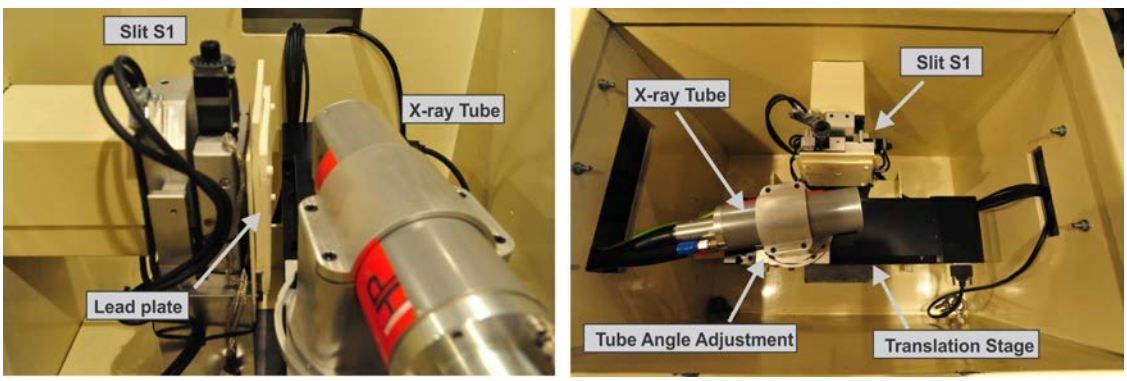

FIG. 4. Side view (left) and top view (right) of the X-ray tube and slit assembly S1, mounted in the source radiation enclosure.

measuring, e.g., 100 mm in length, the 40 μm beam width allows for incidence angles as small as 0.02°, in principle.

The large radiation enclosure housing the goniometer is constructed from wood and is lead-lined on all sides. The large sliding entrance door at the far end of the enclosure is interlocked with the X-ray tube to prevent its operation when the door is open. The radiation enclosure also includes an integrated HEPA filter system arranged to provide vertical laminar flow with minimal particulates, so that sensitive components can be tested without contamination. A lead-covered baffle is located above the top entrance of the HEPA filter, providing an input path for air while blocking any scattered radiation. Specially designed louvered air vents, constructed from lead and steel, are located on two sides at the base of the radiation enclosure so as to provide an exit path for air, again while blocking any scattered radiation. (One vent is visible in the photo shown in Fig. 2.) The large radiation enclosure is estimated to weigh approximately 26 000 kg; it is embedded in a steel-reinforced concrete pad that was installed in the existing concrete floor of the laboratory, directly over an underlying structural steel beam.

Slit assemblies S2 and S3 are located on either side of the goniometer and spaced 910 mm apart (i.e., when S3 is positioned in line with S1 and S2). They are identical to S1, but each includes an additional motorized stage (Huber[18] model 5202.2) for rotation of the slit assembly about the X-ray beam axis. This extra rotational degree of freedom enables all three slits to be precisely co-aligned about the beam axis so as to maximize X-ray flux and maintain a uniformly rectangular beam shape. A high-resolution, stepper-motor-driven goniometer (Huber model 430/440) provides independent rotation of the sample ("TH") and the detector ("TTH") about the vertical direction, with resolution of 0.005° rotation/full-step for both. A "Chi" circle (Huber model 512) is mounted to the TH stage, and a "Phi" stage (Huber model 410) that was already integrated into the 4-circle goniometer has been retained but is not used. The sample mounting assembly is cantilevered to one side of the Chi stage and is shown in more detail in the 3D CAD model shown in Fig. 5. It comprises a porous ceramic vacuum chuck (Tru-Stone Technologies[19]) to hold the sample flat during measurements and two motorized linear stages for sample positioning in both the horizontal (Newport model M-ILS100) and vertical (Newport model M-ILS150) directions, each with 1 μm resolution, and 100 mm and 150 mm of travel, respectively. The vacuum chuck can accommodate samples as large as 150 mm × 150 mm, and the vertical motion enables coating uniformity of test mirrors to be determined as a function of position in the vertical direction. The goniometer assembly is fitted with four (Huber) air-pads and is mounted on a granite block measuring 750 mm × 750 mm × 75 mm; when the air pads are engaged, a small manual linear stage is used to precisely position the goniometer relative to the X-ray beam axis during system alignment. The slit and goniometer stepper motors (and the three linear stages) are controlled using four multi-axis motion controllers (Newport model XPS) that provide 1/10th-step resolution. X-rays are captured by an energy-sensitive, thermoelectrically cooled CdTe detector and preamp[20] (Amptek[21] model XR-100T-CdTe, with 9 mm^2 sensor), mounted directly behind slit assembly S3. A separate electronics unit (Amptek model PX5) provides digital pulse processing, a multi-channel analyzer, and all necessary detector power supplies.

Custom software for instrument control and data acquisition was developed using the IDL programming language (Exelis Visual Information Solutions[22]), on a computer running the CentOS version of the linux operating system. The software controls the X-ray generator, the motor controllers, and the detector electronics. Communications to the motor controllers occur directly via Ethernet, while Ethernet-to-RS232 converters (National Instruments[23] model ENET-232/4) are used to communicate with the X-ray generator and detector electronics. Low-level instrument control is performed using code written in the Python programming language and is called from IDL through its "SPAWN" procedure. A vendor-supplied Python library is used for communications with the motion controllers, while the "PyVISA" Python language package is used in conjunction with the NI-VISA (National Instruments) package for communication with the Ethernet-to-RS232 converters. The top-level IDL software uses a full graphical user interface and has provisions for easily generating and storing automated instrument control and data acquisition sequences, e.g., for sample alignment, slit alignment, and reflectance

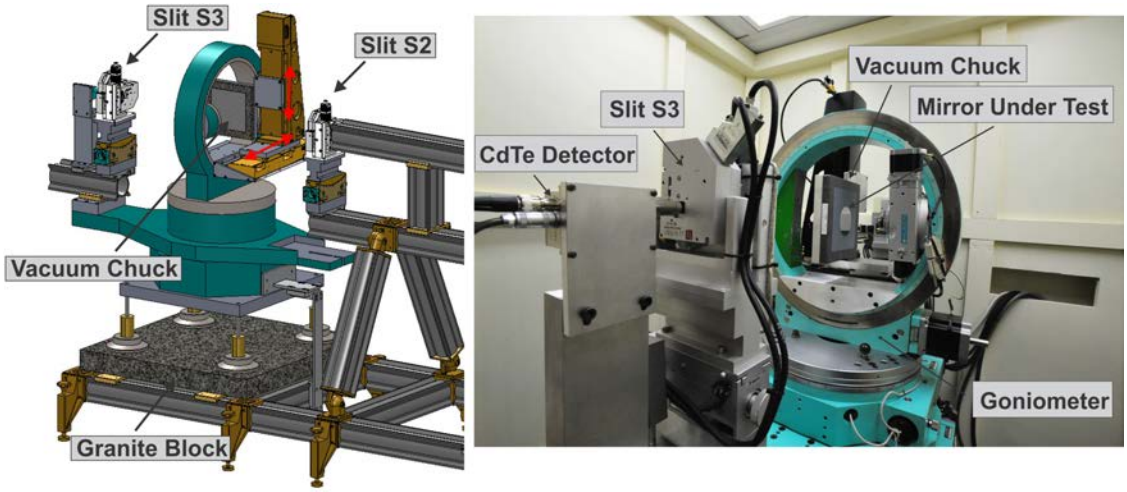

FIG. 5. 3D CAD model (left) and photograph (right) of the goniometer, vacuum chuck, and slits S2 and S3, located inside the HEPA-filtered radiation enclosure.

measurements. Data acquisition and current system configuration parameters are automatically recorded in a master log file after execution of each measurement sequence, so that past measurements and system configurations are easily retrievable.

The energy scale of the X-ray spectrum recorded by the CdTe detector is calibrated using the known energies of emission lines from a small ^{241}Am source. The raw X-ray spectrum recorded by this detector includes K_α and K_β escape peaks from both Cd and Te, at 23.2 and 26.1 keV for Cd and 27.5 and 31.0 keV for Te, respectively.[24] These peaks are due to the escape of secondary X-rays produced in the detector by the interaction of incident X-rays with Cd or Te and result in a distorted spectrum. To address this distortion, an escape-peak correction algorithm was developed (CrossRoads Scientific[25]) and incorporated into the IDL data acquisition software. This algorithm uses the "stripping" procedure described in Ref. 24, where the energy spectrum histogram is corrected channel-by-channel, using values for the needed escape probabilities as a function of incident energy, which were previously determined empirically for the CdTe detector. Fig. 3 shows both corrected and uncorrected spectra.

INSTRUMENT ALIGNMENT AND PERFORMANCE

Initial coarse alignment of the X-ray tube and the three slit assemblies was achieved using a small HeNe laser positioned outside of the radiation enclosure and directed towards the X-ray tube. Coarse alignment of the goniometer relative to the beam axis, and more refined alignment of the slit assemblies, was then achieved visually, using a theodolite in place of the laser. Finally, the X-ray tube and detector were used for precise alignment and calibration of the slit positions, a procedure that can be repeated periodically as necessary. That is, starting with slit S1, and with a relatively small gap between a given pair of slits, the integrated intensity is measured (with S2 and S3 wide open) as the slit-pair gimbal is systematically varied, in order to find the position of maximum flux. With the gimbal positioned at the position of maximum flux, the gap distance is then systematically reduced until the intensity falls linearly to zero, thereby establishing the slit-pair gap origin. The slit pair is finally centered on the X-ray beam. The process is repeated for each of the six slit-pairs. Once the slit assemblies were aligned, the tube angle was adjusted in order to find that angle that provides maximum X-ray intensity. The variation in intensity was found to be small over a region of ~15° centered on the tube normal. Consequently, the tube was finally positioned near normal to the entrance slit S1.

Using a flat X-ray mirror sample mounted on the vacuum chuck, the goniometer was aligned following an iterative procedure, as follows. With the TH stage nominally set for a grazing incidence angle of 0°, the horizontal position of the sample was adjusted (using the horizontal linear stage) until the integrated X-ray intensity was reduced by one half. The TH stage was then rotated by 180° and the intensity was re-measured. The horizontal position of the sample relative to the goniometer and the horizontal position of the goniometer relative to the beam axis were both iteratively adjusted until the beam intensity was halved and equaled for both the TH = 0° and the TH = 180° positions. In this way, the center of the goniometer was positioned to precisely intersect the X-ray beam (to within ±1 μm), and the origin of the horizontal linear stage relative to the goniometer was established (also to within ±1 μm), i.e., the position where the plane of the vacuum chuck mounting surface intersects with the X-ray beam axis (and thus the center of the goniometer).

With the system aligned, reflectance measurements of multilayer mirrors are performed by first recording the incident X-ray spectrum, i.e., with the sample positioned horizontally out of the beam and the detector position at TTH = 0, and then recording the reflected spectrum at the desired incidence angle TH, with the detector positioned at TTH = 2 × TH. The absolute specular reflectance is computed as the ratio of the reflected spectrum to the incident spectrum.

As an example, shown in Fig. 6 is a set of reflectance measurements made using a periodic W/Si multilayer (d = 4.2 nm, N = 80 bilayers) at six different grazing incidence angles ranging from TH = 0.1° to TH = 0.5°, as noted. For clarity, only data in the vicinity of the first order Bragg peaks are shown. The tube was operated at the maximum allowable power with the 0.4 mm focal spot for these measurements: the tube voltage was set to either 160 kV and 5 mA or 40 kV and 15.5 mA. That is, for larger incidence angles, where the first order Bragg peak occurs below ~35 keV, the tube was operated at 40 kV, for maximum flux at low energies; for smaller incidence angles, the tube was operated at 160 kV. With S1 set to 40 μm horizontal × 100 μm vertical, S2 set to 40 μm × 800 μm, and S3 set to 100 μm × 1000 μm, the incident X-ray beam had an integrated intensity of ~5000 cps for the 160 kV tube voltage, with a detector dead-time of less than 2%. The count rate fell to ~3000 cps at the 40 kV tube voltage. An integration time of 15 min was used for both the incident and reflected spectrum measurements, resulting in acceptably low signal-to-noise and a dynamic range of over 3 orders of magnitude. (The detector background count rate was measured to be less than 0.001 cps.) No effort was made to account for non-specular scattered light in these or any other measurements described here; for high-quality multilayer films with relatively low interfacial roughness, the intensity of non-specular scattered light will be several orders of magnitude lower than the intensity of specularly reflected light and will thus have a negligible effect on the measured reflectance.

Also shown in Fig. 6 are the calculated reflectance curves corresponding to each measured curve. The CdTe detector system has finite energy resolution that falls with increasing energy. To account for this, the calculated reflectance curves (computed using IMD[26]) were convolved with a Gaussian whose half-width ranged from 0.25 keV for the measurement made at 0.5°, where the first order Bragg peak is positioned near 30 keV, to 1.5 keV for the measurement made at 0.1°, where the first order Bragg peak is positioned near 85 keV, in rough accord with the variation in energy resolution of the detector as a function of energy as specified by the vendor, and as confirmed experimentally with the ^{241}Am source used for absolute energy calibration. The agreement between measurement and calculation nevertheless begins to breakdown for measurements made at 0.12° and 0.1°, in this case as a result of the imperfect flatness of the coated Si wafer substrate. These

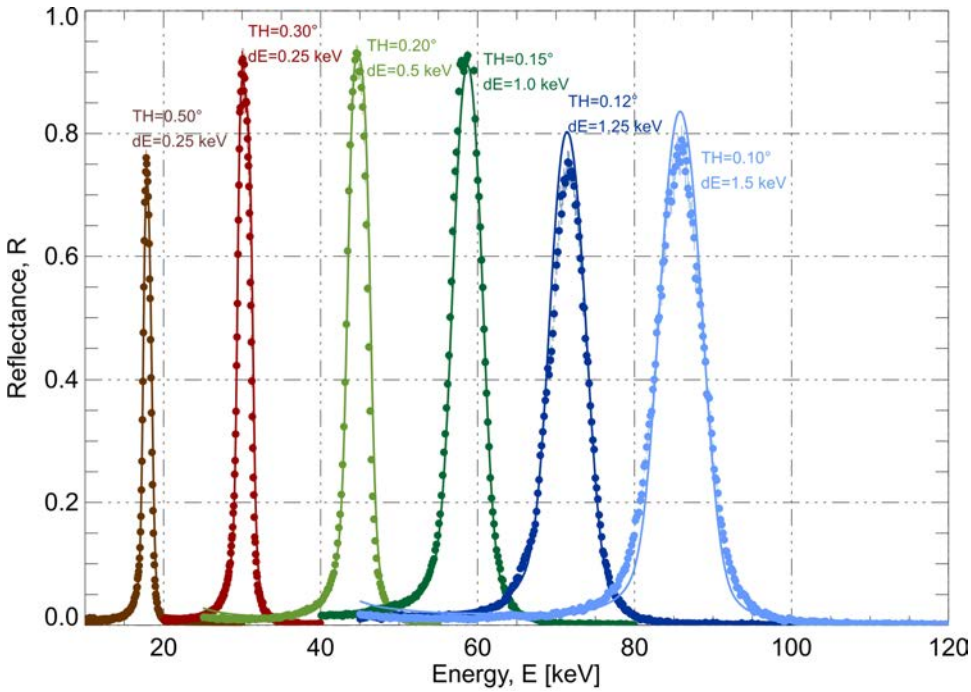

FIG. 6. Reflectance vs. energy of a periodic W/Si multilayer measured at the incidence angles indicated. Calculated reflectance curves are shown as solid lines. The measurements were made using 15 min integration times.

substrates were not optically flat, and the flatness imperfections were not sufficiently corrected through the use of the vacuum chuck during the measurement.

Longer integration times can be used to increase the measurement signal-to-noise ratio and dynamic range, if necessary. For example, shown in Fig. 7 is the reflectance (plotted using a logarithmic scale) vs. energy of the same periodic W/Si multilayer shown in Fig. 6, but in this case measured at one incidence angle (TH = 0.51°), using an integration time of 8 h for acquisition of both the incident and reflected spectra. For this measurement, where the first two Bragg peaks both occur below 40 keV, the tube was operated at 40 kV and 15.5 mA. After a 15 min warm-up, no significant drift in the tube output was observed over the course of the 16 h measurement. For the measurement shown in Fig. 5, the dynamic range has increased to nearly five orders of magnitude as a result of the longer integration time and low detector background. Comparing the measurement to the calculated response (using an energy resolution of 0.276 keV), reasonably good (but imperfect) agreement between the two curves is evident. The higher dynamic

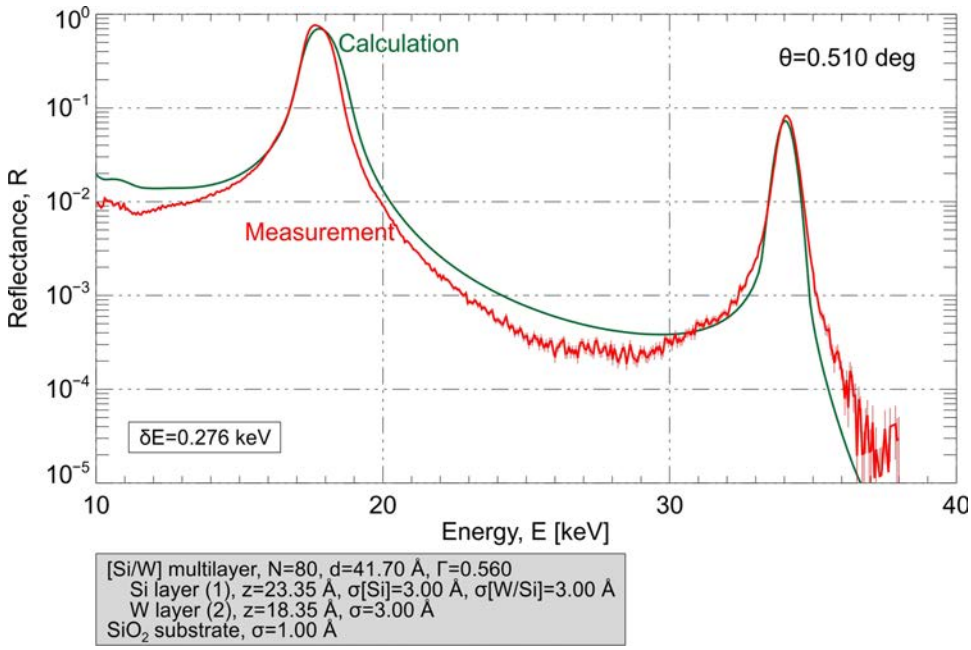

FIG. 7. Reflectance vs. energy at an incidence angle of 0.51° of the W/Si multilayer shown in Fig. 6, using an 8-h integration time for increased signal-to-noise and dynamic range.

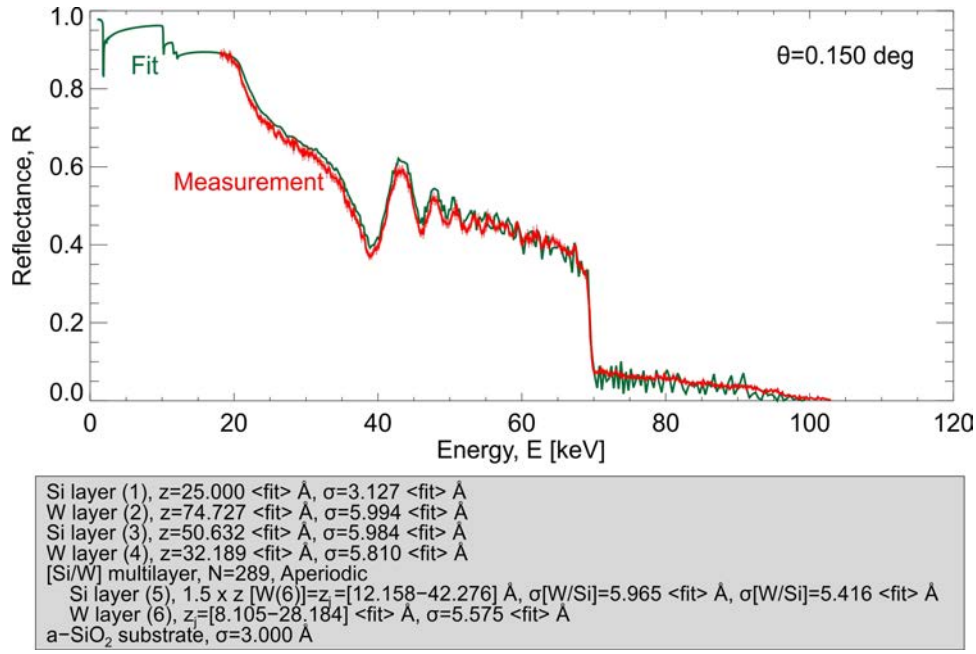

FIG. 8. Measured reflectance vs. energy at an incidence angle of 0.15° for a depth-graded W/Si multilayer. The measurement was made using 15 min integration times for both the incident and reflected spectra. A non-linear least-squares fit to the data is also shown, with the fit parameters indicated.

range obtained using long integration times might be sufficient for non-specular scattering measurements, depending on the scattered light intensity, although such measurements have not yet been pursued.

As a final example, shown in Fig. 8 is the measured reflectance of a depth-graded W/Si multilayer coating designed to provide high reflectance over a broad spectral band up to the W K edge near 70 keV. This particular coating, developed in support of the NuSTAR X-ray telescope,[5] contains 291 bilayers, with bilayer thicknesses ranging from ~2 nm to ~10 nm following a power-law distribution. The reflectance was measured at TH = 0.15°, using a 15 min integration time. Data below 30 keV were obtained using a tube voltage of 40 kV, while data above 30 keV were obtained using a tube voltage of 160 kV. Also shown in Fig. 8 is a non-linear least-squares fit to the measured data, with layer thicknesses and interface widths designated as fit parameters. The agreement between measurement and calculation is excellent (although with so many adjustable fit parameters and with no effort made in the fit to account for the finite, energy-dependent energy resolution of the detector, the significance of this agreement is unclear).

SUMMARY

The development of a laboratory-based X-ray reflectometer to measure the performance of hard X-ray multilayer coatings at their operational X-ray energies and incidence angles has been described. The instrument uses a 160 kV sealed-tube X-ray source with a tungsten anode to provide usable radiation in the 15–150 keV energy band. Motorized tungsten carbide slit assemblies are used to produce a low-divergence pencil beam. Multilayer coatings under test are held flat using a vacuum chuck and are mounted at the center of a high-resolution goniometer used for precise angular positioning of the sample and detector about a vertical axis; additionally, motorized linear stages provide both vertical and horizontal adjustments of the sample position relative to the incident beam. A CdTe energy-sensitive detector is used in conjunction with pulse-shaping electronics and a multi-channel analyzer to capture both the incident and reflected spectra; the absolute reflectance of the coating under test is computed from the ratio of the two (escape-peak-corrected) spectra. The instrument is easy to use and provides rapid performance feedback in the 15–150 keV range that is invaluable during development of hard X-ray multilayer coatings. The system is also well suited for absolute calibration measurements of working multilayer optics and, in principle, could be configured for other types of measurements of X-ray optical components (e.g., filters and gratings) that require a well-defined, small diameter white beam.

ACKNOWLEDGMENTS

This research was funded by NASA, through Grant Nos. NNX09AC45G and NNX13AC54G.

[1]K. D. Joensen, P. Høghøj, F. E. Christensen, P. Gorenstein, J. Susini, E. Ziegler, A. K. Freund, and J. L. Wood, "Multilayers supermirror structures for hard x-ray synchrotron and astrophysics instrumentation," Proc. SPIE **2001**, 360 (1994).
[2]K. D. Joensen, P. Voutov, A. Szentgyorgyi, J. Roll, P. Gorenstein, P. Høghøj, and F. E. Christensen, "Design of grazing-incidence multilayer supermirrors for hard-x-ray reflectors," Appl. Opt. **34**, 7935 (1995).
[3]A. Rack, T. Weitkamp, M. Riotte, D. Grigoriev, T. Rack, L. Helfen, T. Baumbach, R. Dietsch, T. Holz, M. Krämer, F. Siewert, M. Meduna, P. Cloetens, and E. Ziegler, "Comparative study of multilayers used in monochromators for synchrotron-based coherent hard x-ray imaging," J. Synchrotron Radiat. **17**, 496 (2010).
[4]D. L. Windt, F. E. Christensen, W. W. Craig, C. Hailey, F. A. Harrison, M. Jimenez-Garate, R. Kalyanaraman, and P. H. Mao, "Growth, structure

and performance of depth-graded W/Si multilayers for hard x-ray optics," J. Appl. Phys. **88**, 460–470 (2000).
[5]F. E. Christensen, A. C. Jakobsen, N. F. Brejnholt, K. K. Madsen, A. Hornstrup, N. J. Westergaard, J. Momberg, J. Koglin, A. M. Fabricant, M. Stern, W. W. Craig, M. J. Pivovaroff, and D. Windt, "Coatings for the NuSTAR mission," Proc. SPIE **8147**, 81470U (2011).
[6]D. L. Windt, S. Donguy, C. J. Hailey, J. Koglin, V. Honkimaki, E. Ziegler, F. E. Christensen, C. M. H. Chen, F. A. Harrison, and W. W. Craig, "W/SiC x-ray multilayers optimized for use above 100 keV," Appl. Opt. **42**, 2415 (2003).
[7]M. Fernández-Perea, M. J. Pivovaroff, R. Soufli, J. Alameda, P. Mirkarimi, M.-A. Descalle, S. L. Baker, T. McCarville, K. Ziock, D. Hornback, S. Romaine, R. Brunic, Z. Zhong, V. Honkimäki, E. Ziegler, F. E. Christensen, and A. C. Jakobsen, "Ultra-short-period WC/SiC multilayer coatings for x-ray applications," Nucl. Instrum. Methods Phys. Res., Sect. A **710**, 114 (2013).
[8]N. F. Brejnholt, R. Soufli, M.-A. Descalle, M. Fernández-Perea, F. E. Christensen, A. C. Jakobsen, V. Honkimäki, and M. J. Pivovaroff, "Demonstration of multilayer reflective optics at photon energies above 0.6 MeV," Opt. Express **22**, 15364 (2014).
[9]P. Høghøj, K. Joensen, F. E. Christensen, J. Susini, E. Ziegler, A. K. Freund, E. Lüken, and C. Riekel, "Measurement of multilayer reflectivities from 8 keV to 130 keV," Proc. SPIE **2011**, 354 (1993).
[10]N. F. Brejnholt, F. E. Christensen, A. C. Jakobsen, C. J. Hailey, J. E. Koglin, K. L. Blaedel, M. Stern, D. Thornhill, C. Sleator, S. Zhang, W. W. Craig, K. K. Madsen, T. Decker, M. J. Pivovaroff, and J. K. Vogel, "NuSTAR ground calibration: The Rainwater Memorial Calibration Facility (FaMCaF)," Proc. SPIE **8147**, 81470I (2011).
[11]T. Matsushita, Y. Niwa, Y. Inada, M. Nomura, M. Ishii, K. Sakurai, and E. Arakawa, "High-speed x-ray reflectometry in multiwavelength-dispersive mode," Appl. Phys. Lett. **92**, 024103 (2008).
[12]M. Bhattacharya, M. K. Mukhopadhyay, S. Pal, and M. K. Sanyal, "Energy dispersive x-ray reflectivity to study phase transitions in thin films," Radiat. Phys. Chem. **70**, 611 (2004).
[13]F. Neissendorfer, U. Pietsch, G. Brezesinski, and H. Möhwald, "The energy-dispersive reflectometer/diffractometer at BESSY-I," Meas. Sci. Technol. **10**, 354 (1999).
[14]Comet Technologies USA, Inc., Shelton, CT.
[15]JJ X-Ray A/S, Lyngby, Denmark.
[16]Energy Services, Shelton, CT; Bookholt Associates, Vernon, NJ.
[17]Newport Corporation, Irvine, CA.
[18]HUBER Diffraktionstechnik GmbH & Co. KG, Rimsting, Germany.
[19]Starrett Tru-Stone Technologies Division, Waite Park, MN.
[20]R. H. Redus, A. Huber, J. Pantazis, T. Pantazis, and D. Sperry, "Design and performance of the x-123 compact x-ray and gamma-ray spectroscopy system," *Nuclear Science Symposium Conference Record* (IEEE, 2006), Vol. 6.
[21]Amptek, Inc., Bedford, MA.
[22]Exelis Visual Information Solutions, Inc., Boulder, CO.
[23]National Instruments Corporation, Austin, TX.
[24]R. H. Redus, J. A. Pantazis, T. J. Pantazis, A. C. Huber, and B. J. Cross, "Characterization of CdTe detectors for quantitative x-ray spectroscopy," IEEE Trans. Nucl. Sci. **56**, 2524 (2009).
[25]CrossRoads Scientific, El Granada, CA.
[26]D. L. Windt, "IMD—Software for modeling the optical properties of multilayer films," Comput. Phys. **12**, 360 (1998).